Demetalation of a Dimolybdenum Cyclotetraphosphoxane Cage Complex and Syntheses of Heterobimetallic Cages

Haiying Yang,[†] Edward H. Wong,*[,†] Arnold L. Rheingold,*[,‡] Beth E. Owens-Watermire,[‡] and Brian S. Haggerty[‡]

Departments of Chemistry, University of New Hampshire, Durham, New Hampshire 03824, and University of Delaware, Newark, Delaware 19716

Received June 16, 1994[⊗]

Selective excision of the Mo^{II} vertex in the mixed-valent, adamantanoid cage complex $Mo(CO)_4[^iPr_2NPO]_4Mo(CO)_2I_2$ with sodium dithiocarbamate yielded the metalla ligand $Mo(CO)_4[^iPr_2NPO]_4$ (**1**). Complex **1** has been characterized by spectroscopy and by X-ray crystallography. Its structure retains the parent adamantane framework except for the vacant metal vertex. Significant distortions of the P_4O_4 core are noted with [Mo]–P–O bonds (1.623 (4) Å) shortened at the expense of the uncoordinated P–O bonds (1.671 (4) Å). Nucleophilic attack by primary alcohols (ROH) on **1** led to cleavage of a single P–O–P bond to give $Mo(CO)_4[(^iPr_2NPO)_2(^iPr_2NPOR)\{^iPr_2NP(O)H\}]$ (R = Me, **3a**; R = Et, **3b**); the postulated monocyclic structure of **3a** has been confirmed by X-ray crystallography. Synthetically the covergent lone pairs in **1** enabled formation of new heterobimetallic cage complexes of the type $Mo(CO)_4[^iPr_2NPO]_4M$ (**4a–g**; M = $Cr(CO)_4$, $Fe(CO)_3$, $NiBr_2$, $PtCl_2$, $Cu(MeCN)_2BF_4$, $AgNO_3$, $PdBr_2$). The molecular structure of $Mo(CO)_4[^iPr_2NPO]_4NiBr_2$ (**4c**) has been determined. A pseudotetrahedral coordination geometry was observed at the paramagnetic Ni^{II} center, and the P_4O_4 core was found to have readjusted to its electronic demands. Comparison of the spectral properties of the conserved $Mo(CO)_4$ moiety in these products suggests a small but observable transmission of intracage influence from the heterometal. Treatment of **4c** with iron pentacarbonyl led to reduction of the nickel vertex and formation of the diamagnetic complex $Mo(CO)_4[^iPr_2NPO]_4Ni(CO)_2$ (**6**). Competitive chlorination and iodination of **6** revealed preferential halogenation at the nickel site.

Introduction

The adamantanoid framework has proven to be a pervasive motif in structural chemistry (Figure 1).[1] Selective substitution of one or more vertices can potentially be exploited to produce useful modifications of the basic cage unit. We have previously reported on a family of $M_2P_4O_4$ cage complexes featuring a tetradentate tetraphosphoxane ring chelating two metal vertices to form such a core (Figure 2).[2] The parent $Mo(CO)_4[^iPr_2NPO]_4MO(CO)_4$ complex has been shown to exhibit mixed-valent and intracage oxidative-addition reactions.[3,4] A series of heterobimetallic complexes of this type with rigidly constrained pairs of metal vertices should be especially interesting for the study of intracage metal–metal interactions. Substituted cages of this type, however, have been elusive due to lack of rational synthetic routes.[2] While attempted demetalation of the parent cage complex failed, we note that its mixed-valent derivative $Mo(CO)_4[^iPr_2NPO]_4Mo(CO)_2I_2$ contains one Mo^{II} center which does present a potential decomplexation site.[3] We have now shown that dithiocarbamates can indeed selectively remove this vertex to give the monometallic cage precursor complex $Mo(CO)_4[^iPr_2NPO]_4$ (**1**).[5] Described herein are the synthesis, characterization, and chemistry of this compound, including its use as a metalla ligand for the preparation of heterobimetallic cage complexes.

Results

Synthesis and Characterization of $Mo(CO)_4[^iPr_2NPO]_4$ (1). Reaction of the mixed-valent cage complex $Mo(CO)_4[^iPr_2NPO]_4Mo(CO)_2I_2$ with sodium dimethyldithiocarbamate in methylene chloride at room temperature yielded a red suspension which was filtered to give a red solid subsequently identified as $Mo(CO)_2(S_2CNMe_2)_2$. The filtrate contained two products which can be separated; the white solid complex **1** in 60% yield and an unstable orange solid **2** in varying yields. Complex **1** is air-stable and has IR carbonyl absorption bands at 2023, 1925, 1908, and 1882 cm^{-1} indicative of a *cis*-$Mo(CO)_4$ fragment as well as POP stretches between 838 and 892 cm^{-1} (Table 1). Its proton-decoupled ^{31}P NMR spectrum exhibits one sharp and

[†] University of New Hampshire.
[‡] University of Delaware.
[⊗] Abstract published in *Advance ACS Abstracts,* November 1, 1994.

(1) See, for example: Corbridge, D. E. C. *The Structural Chemistry of Phosphorus*; Elsevier: New York, 1974; Table 56, p 422. Gimarc, B. M.; Ott, J. J. *J. Am. Chem. Soc.* **1986**, *108*, 4298 (Table I).
(2) Wong, E. H.; Turnbull, M. M.; Hutchinson, K. D.; Valdez, C.; Gabe, E. J.; Lee, F. L.; Le Page, Y. *J. Am. Chem. Soc.* **1988**, *110*, 8422.
(3) Turnbull, M. M.; Valdez, C.; Wong, E. H.; Gabe, E. J.; Lee, F. L. *Inorg. Chem.* **1992**, *31*, 208.
(4) Yang, H. Y.; Wong, E. H.; Jasinski, J. P.; Pozdniakov, R. Y.; Woudenberg, R. *Organometallics* **1992**, *11*, 1579.
(5) Preliminary results have been communicated: Yang, H.; Wong, E. H.; Rheingold, A. L.; Owens-Waltermire, B. E. *J. Chem. Soc., Chem. Commun.* **1993**, 35.
(6) Sun, X.; Wong, E. H.; Turnbull, M. M.; Rheingold, A. L.; Watermire, B. E.; Ostrander, R. L. *Organometallics*, in press.

0276-7333/94/2313-4825$04.50/0

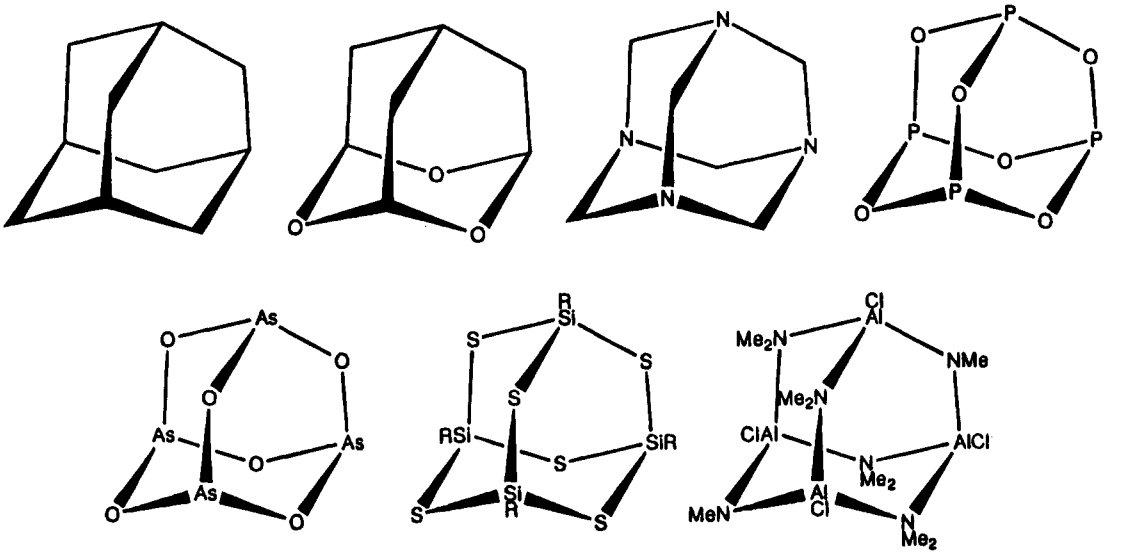

Figure 1. Examples of known compounds with the adamantane cage structure.

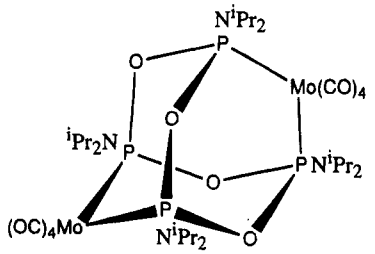

Figure 2. Schematic drawing of the $Mo(CO)_4[^iPr_2NPO]_4Mo(CO)_4$ cage complex.

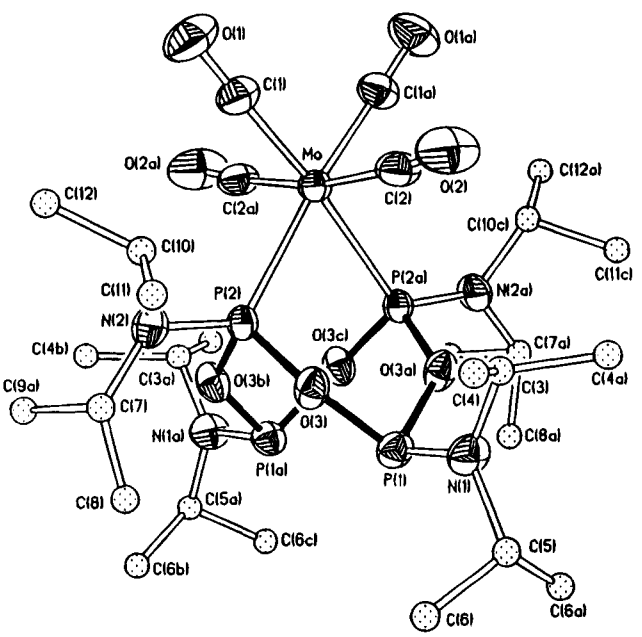

Figure 3. Molecular structure of complex **1**, $Mo(CO)_4[^iPr_2NPO]_4$.

one broad triplet (δ 150.6 and 126.0, $^2J_{POP}$ = 2 Hz, Table 2). In addition, its solid-state molecular structure has been determined by X-ray crystallography to retain the parent adamantane-like cage geometry except for the vacant metal vertex (Figure 3).

Reactions of Complex 1 with Nucleophiles and Alkylating Agents. Excess methanol and ethanol reacted with **1** in methylene chloride solutions to give high yields of the P–O–P cleavage products **3a,b** (eq 1). Their $^{31}P\{^1H\}$ NMR spectra (Table 2) exhibited

$$\mathrm{ROH} + \underset{\mathbf{1}}{\mathrm{Mo(CO)_4[^iPr_2NPO]_4}} \rightarrow \mathrm{Mo(CO)_4[(^iPr_2NPO)_2(^iPr_2NPOR)\{^iPr_2NP(O)H\}]} \quad (1)$$

R = Me (**3a**), Et (**3b**)

ABMX patterns with the proton-coupled spectra showing large $^1J_{PH}$ couplings (>600 Hz) for the upfield X multiplet. Their elemental analyses and an X-ray crystallographic study of **3a** (Figure 4) confirmed the characterization of these monocyclic complexes as products of nucleophilic attack at coordinated P sites with ensuing P–O–P cleavage. Isopropyl alcohol reacted much more sluggishly with further degradation of the cage structure to give aminophosphoryl species. Similarly, secondary amines such as piperidine degraded complex **1** to form *bis*(amino)phosphine oxides.

Attempted alkylations of complex **1** with methyl iodide or benzyl bromide in a variety of solvents were unsuccessful, even after extended reaction times. Similarly, benzaldehyde also failed to react with **1**.

Syntheses of Heterobimetallic Complexes 4a–g and 5a,b from Complex 1. Typically hexane or

Table 1. Infrared Data for Cage Complexes[a]

complex	ν_{CO} (cm^{-1})	ν_{POP} (cm^{-1})
1	2022.8, 1925.1, 1908.1, 1882.5	891.5, 873.5, 860.2, 838.4
2	2018, 1952, 1910, 1890	871, 843
3a	2027.2, 1928.0, 1909.8, 1895.8	895.6, 881.7, 859.4, 845.5
3b	2027.5, 1942.9, 1919.3, 1903.6	896.9, 883.2, 859.6, 839.9
4a	2035.3, 2020.8, 1930.5, 1900.6	879.0, 854.4, 805.3
4b	2021, 2014, 1960, 1937, 1907	867, 847, 795
4c	2036.7, 1946.9, 1936.9, 1899.8	907.2, 861.0, 830.1
4d	2045.1, 1958.7, 1948.1, 1917.6	912.9, 873.0, 847.1, 831.0
4e	2031.3, 1908.0 (broad)	902.9, 885.9, 860.0, 814.1
4f	2029.7, 1936.2, 1908.2	904.8, 887.3, 861.4, 815.0
4g	2045.8, 1961.0, 1943.0, 1921.8	908.9, 871.7, 845.2, 820.1
5a	1981.6, 1910.4, 1880.1	917.8, 888.3, 867.6, 858.9, 834.8
5b	1981.2, 1910.9, 1880.1	916.1, 887.1, 866.4, 858.2, 833.3
6	2022.9, 1968.8, 1931.3, 1919.5, 1905.6	881.3, 854.6, 797.7
7a	2035.7, 1947.4, 1936.3, 1900.0	908.1, 862.1, 831.8
7b	2037.4, 1950.5, 1932.2, 1921.0	904.1, 886.5, 859.6, 823.0

[a] All spectra taken using KBr pellets. FT-IR data are to the nearest 0.1 cm^{-1}.

Table 2. $^{31}P\{^1H\}$ NMR Data for Cage Complexes[a]

complex	chem shift, ppm [*J*, Hz]
$Mo(CO)_4[^iPr_2NPO]_4$ (**1**)	150.6 (t), 126.0 (t, bd) [$^2J = 2$]
$Mo(CO)_4[^iPr_2NPO]_4Mo(CO)_2(S_2CNMe_2)_2$ (**2**)	201.1 (d), 180.5 (d), 154.9 (d), 151.0 (d) [$^2J_{AB} = 146$, $^2J_{XY} = 39$]
$Mo(CO)_4[^iPr_2NPO]_2(^iPr_2NPOMe)\{^iPr_2NP(O)H\}$ (**3a**)	169.1 (d of d), 154.4 (d of d of d), 131.3 (d of d), −1.50 (d) [^2J: AB = 34, AM = 92, BM = 111, BX = 32, $^1J_{PH} = 635$ (proton coupled)]
$Mo(CO)_4[^iPr_2NPO]_2(^iPr_2NPOEt)\{^iPr_2NP(O)H\}$ (**3b**)	164.4 (d of d), 153.1 (d of d of d), 131.2 (d of d), −2.9 (d) [^2J: AB = 34, AM = 98, BM = 115, BX = 29, $J_{PH} = 641$ (proton coupled)]
$Mo(CO)_4[^iPr_2NPO]_4Cr(CO)_4$ (**4a**)	175.0 (t), 147.9 (t) [$^2J = 6$]
$Mo(CO)_4[^iPr_2NPO]_4Fe(CO)_3$ (**4b**)	165.2 (t), 152.1 (t) [$^2J = 14$]
$Mo(CO)_4[^iPr_2NPO]_4NiBr_2$ (**4c**)	paramagnetic
$Mo(CO)_4[^iPr_2NPO]_4PtCl_2$ (**4d**)	147.4 (t), 132.6 (t), 56.5 (t), −19.4 (t) [$^2J = 10$, $^1J_{PtP} = 5520$]
$Mo(CO)_4[^iPr_2NPO]_4Cu(MeCN)_2BF_4$ (**4e**)	155.6 (t), 90.9 (t, bd) [$^2J = 10$]
$Mo(CO)_4[^iPr_2NPO]_4AgNO_3$ (**4f**)	154.3 (t), 103.6 and 103.5 (d of t, $^2J = 13$ Hz, $^1J_{AgP} = 568$ and 492]
$Mo(CO)_4[^iPr_2NPO]_4PdBr_2$ (**4g**)	147.6 (t), 82.6 (t) [$^2J = 6$]
$Mo(CO)_3[^iPr_2NPO]_5PdCl_2$ (**5a**)	154.7 (t of t), 134.9 (d), 86.0 (d) [$^2J_{AM} = 30$, $^2J_{AX} = 11$]
$Mo(CO)_3[^iPr_2NPO]_5PdBr_2$ (**5b**)	154.0 (t of t), 134.7 (d), 85.4 (d) [$^2J_{AM} = 30$, $^2J_{AX} = 10$]
$Mo(CO)_4[^iPr_2NPO]_4Ni(CO)_2$ (**6**)	154.5 (t), 128.0 (t) [$^2J = 3$]
$Mo(CO)_4[^iPr_2NPO]_4NiCl_2$ (**7a**)	paramagnetic
$Mo(CO)_4[^iPr_2NPO]_4NiI_2$ (**7b**)	paramagnetic

[a] Spectra were run in $CDCl_3$ solutions (d = doublet, t = triplet, bd = broad).

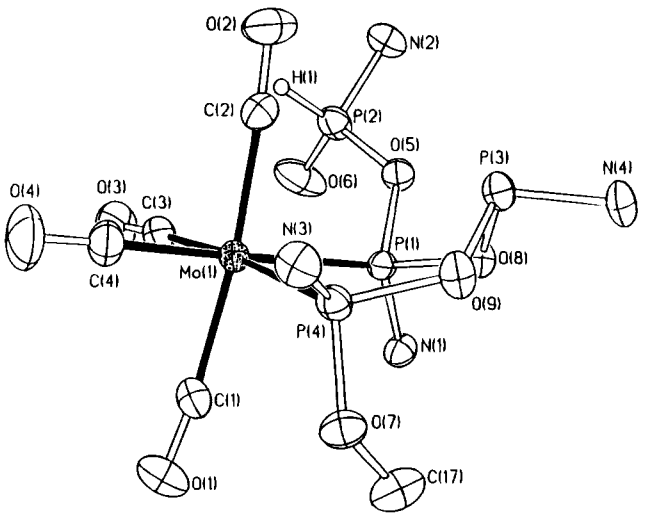

Figure 4. Molecular structure of complex **3a**, $Mo(CO)_4[(^iPr_2NPO)_2(^iPr_2NPOMe)\{^iPr_2NP(O)H\}]$, with diisopropyl groups on nitrogens omitted for clarity.

hexane/methylene chloride solutions of complex **1** were refluxed with the respective heterometal precursors, including $Cr(CO)_4(NBD)$, $Fe_2(CO)_9$, $NiBr_2(DME)$, $PtCl_2(NBD)$, and $Cu(MeCN)_4BF_4$ (**4a–e**, Scheme 1). The silver nitrate complex **4f** was prepared in the dark, while chromatography was necessary for the isolation of pure samples of complexes **4a,b**. All except the silver complex **4f** are air-stable solids that gave satisfactory elementary analyses. Their spectral data are listed in Tables 1 and 2. Additionally, the molecular structure of the Mo/Ni complex **4c** has been determined (Figure 5) to confirm the formation of a heterobimetallic cage.

Attempted synthesis of a MoP_4O_4Pd cage complex was carried out. From **1** and $PdCl_2$·2PhCN, the major isolated product was a light yellow solid with only three carbonyl IR stretches at 1982, 1910, and 1880 cm^{-1} indicative of a fac-$Mo(CO)_3$ fragment. Its $^{31}P\{^1H\}$ NMR spectrum exhibited an AMM′XX′ pattern (Table 2), suggesting a pentaphosphorus donor set. Elemental analyses were also consistent with the formulation of this complex as $Mo(CO)_3[^iPr_2NPO]_5PdCl_2$ (**5a**) (Figure 6). Similarly, reaction of complex **1** with $PdBr_2$·2PhCN in toluene at 70 °C for 72 h resulted in the formation of a MoP_5O_5Pd cage (**5b**) along with smaller yields of the desired $Mo(CO)_4[^iPr_2NPO]_4PdBr_2$ complex **4g**. Decreasing the reaction time to 16 h allowed isolation of **4g** as the major product in over 80% yield (eq 2).

$$\underset{\mathbf{1}}{Mo(CO)_4[^iPr_2NPO]_4} + PdBr_2\cdot 2PhCN \rightarrow \underset{\mathbf{4g}}{Mo(CO)_4[^iPr_2NPO]_4PdBr_2} + 2PhCN \quad (2)$$

Synthesis and Halogenation Reactions of $Mo(CO)_4[^iPr_2NPO]_4Ni(CO)_2$ (6). In refluxing hexane, $Fe(CO)_5$ reduced and carbonylated the Ni^{II} vertex of **4g** to give complex **6** as a white solid in 85% yield. Use of $Fe_2(CO)_9$ led to similar results. Complex **6** exhibited carbonyl IR bands at 2023, 1969, 1931, 1920, and 1906 cm^{-1} and the expected AA′XX′ pattern in its $^{31}P\{^1H\}$ NMR spectrum (Tables 1 and 2), consistent with its formulation as $Mo(CO)_4[^iPr_2NPO]_4Ni(CO)_2$. Competitive halogenation of **6** using elemental iodine or sulfuryl chloride resulted in exclusive reaction at the Ni vertex to give $Mo(CO)_4[^iPr_2NPO]_4NiX_2$ (X = Cl (**7a**), I (**7b**)) (eq 3).

$$I_2 + \underset{\mathbf{6}}{Mo(CO)_4[^iPr_2NPO]_4Ni(CO)_2} \rightarrow \underset{\mathbf{7b}}{Mo(CO)_4[^iPr_2NPO]_4NiI_2} + 2CO \quad (3)$$

Molecular Structure of Complex 1. The molecular structure of $Mo(CO)_4[^iPr_2NPO]_4$ (**1**) is shown in Figure 3. Except for the vacant molybdenum vertex, the basic geometry of the parent MoP_4O_4Mo core is retained. The metal–phosphorus distance is 2.512(2) Å. Two kinds of disparate core P–O bond lengths are noted. Those still bonded to Mo are shorter at 1.623(4) Å (P(2)–P(3)), while the uncoordinated P–O lengths are elongated to 1.671(4) Å (P(1)–O(3)). Metal–carbonyl distances cis to phosphorus are slightly longer (2.027(10) Å) than the trans Mo–C bonds (1.987(9) Å). The distorted-octahedral coordination sphere around the remaining Mo center features a slightly nonlinear C(2)–Mo–C(2a) angle of 169.8(5)°, a P–Mo–P angle of 75.1(1)°, and a near-orthogonal C(1)–Mo–C(1a) angle of 87.5(5)°. Two types of core O–P–O angles are also observed; those at coordinating P(2) and P(2a) being larger at 102.1(3)° compared to those at P(1) and P(1a) at 97.3(3)°. Other selected bond distances and angles are listed in Table 3.

Scheme 1

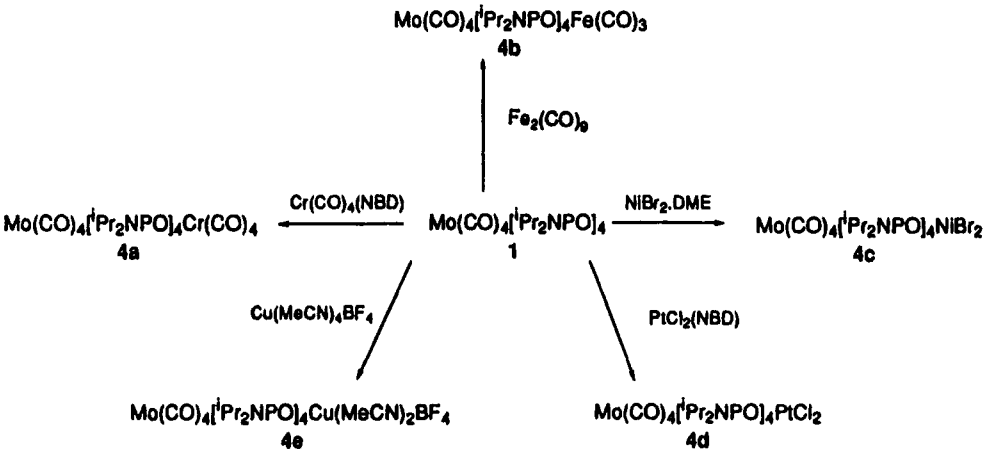

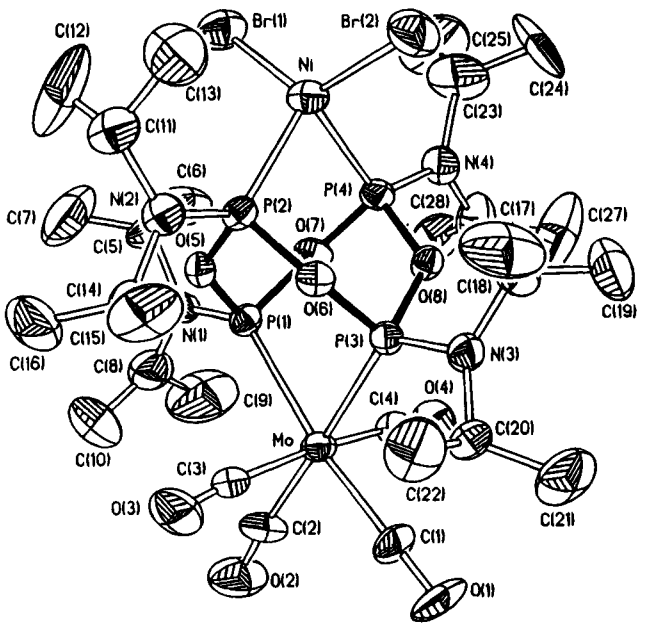

Figure 5. Molecular structure of complex **4c**, $Mo(CO)_4[^iPr_2NPO]_4NiBr_2$.

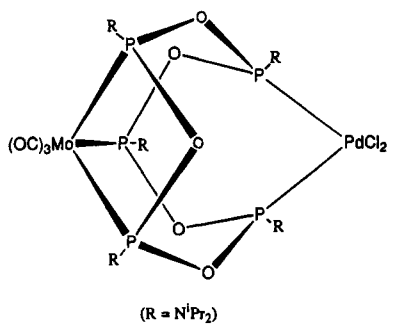

Figure 6. Proposed structure of complex **5a**, $Mo(CO)_3[^iPr_2NPO]_5PdCl_2$.

Molecular Structure of Complex 3a. The molecular structure of $Mo(CO)_4[(^iPr_2NPO)_2(^iPr_2NPOMe)\{^iPr_2NP(O)H\}]$ (**3a**) is shown in Figure 4. Cleavage of one Mo-coordinated P–O bond by methanol has occurred with inversion at P(4). A single Mo–P(4)–O(9)–P(3)–O(8)–P(1) chelate ring remains and is in a flattened-boat conformation. Within this heterocycle, Mo–P distances are 2.521(2) and 2.501(2) Å for Mo–P(1) and Mo–P(4), respectively. Again, two types of P–O bonds are noted; the [Mo]–P–O lengths are shorter at 1.616(3)–1.644(3) Å, while the remaining P–O's range from 1.649(3) to 1.679(3) Å. With relief of the polycyclic strain, the P(1)–Mo–P(4) angle has opened up to near-orthogonality (89.1(1)°) from the value of 75.1(1)° in the parent complex **1**. As expected, axial Mo–carbonyl bonds are slightly longer (2.030(5) Å) compared to equatorial Mo–C's (1.995(6) Å). A tabulation of other selected bond distances and angles is presented in Table 4.

Table 3. Selected Bond Distances and Angles for Complex 1

Bond Distances (Å)			
Mo–P(2)	2.512(2)	Mo–C(1)	1.978(9)
Mo–C(2)	2.027(10)	P(1)–O(3)	1.671(4)
P(1)–N(1)	1.655(6)	P(2)–O(3)	1.623(4)
P(2)–N(2)	1.642(7)	C(1)–O(1)	1.167(11)
C(2)–O(2)	1.143(12)		
Bond Angles (deg)			
P(2)–Mo–C(1)	98.7(3)	P(2)–Mo–C(2)	94.0(2)
C(1)–Mo–C(2)	86.3(2)	P(2)–Mo–P(2A)	75.1(1)
C(1)–Mo–P(2A)	173.8(3)	C(1)–Mo–C(1A)	87.5(5)
C(2)–Mo–C(1A)	86.3(2)	P(2A)–Mo–C(1A)	98.7(3)
C(2)–Mo–C(2A)	169.8(5)	O(3)–P(1)–O(3B)	97.3(3)
Mo–P(2)–O(3)	112.1(1)	O(3)–P(2)–O(3A)	102.1(3)
P(1)–O(3)–P(2)	131.6(2)		

Molecular Structure of Complex 4c. The heterobimetallic complex $Mo(CO)_4[^iPr_2NPO]_4NiBr_2$ (**4c**) has the cage structure shown in Figure 5. The MoP_4O_4Ni framework features the tetraphosphoxane core in a boat–boat form chelating both metal vertices. Molybdenum–phosphorus distances are both 2.493(4) Å, while nickel–phosphorus bonds are shorter at 2.254(4) and 2.266(4) Å. Phosphorus–oxygen bond lengths at Mo-coordinated sites range from 1.639(9) to 1.661(9) Å, while those coordinated to Ni span 1.627(8)–1.654(9) Å. Angles around the metals are 77.9(1)° for P(1)–Mo–P(3) and 85.7(1)° for P(2)–Ni–P(4). Two ranges of O–P–O angles are observed; at Mo-coordinated sites slightly smaller values of 98.4–98.9(4)° are found, while at Ni sites they are 100.6–100.7(4)°. Framework P–O–P angles vary from 127.8(5) to 133.6(5)°.

The coordination geometry about nickel is approximately C_{2v} with a large Br(1)–Ni–Br(2) angle of 128.9(1)° and a pinched P(2)–Ni–P(4) angle of 85.7(1)°. In contrast, all P–Ni–Br angles are close to tetrahedral (106.4(1)–111.3(1)°). The coordination geometry around the molybdenum center is essentially unchanged from that in complex **1** and the parent $Mo(CO)_4[^iPr_2NPO]_4Mo$-

Table 4. Selected Bond Distances and Angles for Complex 3a

Bond Distances (Å)			
Mo(1)–P(1)	2.521(2)	Mo(1)–P(4)	2.501(2)
Mo(1)–C(1)	2.029(5)	Mo(1)–C(2)	2.030(5)
Mo(1)–C(3)	1.998(5)	Mo(1)–C(4)	1.992(6)
P(1)–O(5)	1.668(3)	P(1)–O(8)	1.616(3)
P(1)–N(1)	1.644(4)	P(2)–O(5)	1.604(3)
P(2)–O(6)	1.452(5)	P(2)–N(2)	1.609(4)
P(3)–O(8)	1.679(3)	P(3)–O(9)	1.649(3)
P(3)–N(3)	1.648(4)	P(4)–O(7)	1.602(3)
P(4)–O(9)	1.644(3)	P(4)–N(3)	1.655(4)
O(1)–C(1)	1.144(7)	O(2)–C(2)	1.145(6)
O(3)–C(3)	1.142(7)	O(4)–C(4)	1.142(7)
O(7)–C(17)	1.422(6)		
Bond Angles (deg)			
P(1)–Mo(1)–P(4)	89.1(1)	P(1)–Mo(1)–C(1)	98.3(2)
P(4)–Mo(1)–C(1)	87.1(2)	P(1)–Mo(1)–C(2)	88.7(1)
P(4)–Mo(1)–C(2)	92.2(1)	C(1)–Mo(1)–C(2)	172.9(2)
P(1)–Mo(1)–C(3)	92.3(2)	P(4)–Mo(1)–C(3)	175.5(1)
C(1)–Mo(1)–C(3)	88.4(2)	C(2)–Mo(1)–C(3)	92.1(2)
P(1)–Mo(1)–C(4)	177.8(2)	P(4)–Mo(1)–C(4)	91.0(2)
C(1)–Mo(1)–C(4)	83.9(2)	C(2)–Mo(1)–C(4)	89.1(2)
C(3)–Mo(1)–C(4)	87.8(2)	Mo(1)–P(1)–O(5)	113.4(1)
O(5)–P(1)–O(8)	95.6(2)	O(5)–P(2)–O(6)	113.5(2)
O(8)–P(3)–O(9)	96.5(2)	O(7)–P(4)–O(9)	99.0(2)
P(1)–O(5)–P(2)	131.5(2)	P(1)–O(8)–P(3)	121.8(2)
P(3)–O(9)–P(4)	125.1(2)		

Table 5. Selected Bond Distances and Angles for Complex 4c

Bond Distances (Å)			
Mo–P(1)	2.493(4)	Mo–P(3)	2.493(4)
Mo–C(1)	2.004(15)	Mo–C(2)	1.987(17)
Mo–C(3)	2.047(17)	Mo–C(4)	2.019(17)
Ni–Br(1)	2.320(3)	Ni–Br(2)	2.318(3)
Ni–P(2)	2.254(4)	Ni–P(4)	2.266(4)
P(1)–O(5)	1.639(9)	P(1)–O(7)	1.661(9)
P(1)–N(1)	1.587(11)	P(2)–O(5)	1.654(9)
P(2)–O(6)	1.627(8)	P(2)–N(2)	1.614(12)
P(3)–O(6)	1.653(9)	P(3)–O(8)	1.649(9)
P(3)–N(3)	1.660(11)	P(4)–O(7)	1.623(9)
P(4)–O(8)	1.631(8)	P(4)–N(4)	1.609(12)
O(1)–C(1)	1.125(19)	O(2)–C(2)	1.162(21)
O(3)–C(3)	1.140(21)	O(4)–C(4)	1.130(21)
Bond Angles (deg)			
P(1)–Mo–P(3)	77.9(1)	P(1)–Mo–C(1)	171.9(4)
P(3)–Mo–C(1)	96.4(4)	P(1)–Mo–C(2)	100.8(5)
P(3)–Mo–C(2)	177.7(4)	C(1)–Mo–C(2)	85.2(6)
P(1)–Mo–C(3)	94.3(4)	P(3)–Mo–C(3)	92.2(5)
C(1)–Mo–C(3)	91.6(6)	C(2)–Mo–C(3)	85.9(6)
P(1)–Mo–C(4)	89.0(4)	P(3)–Mo–C(4)	94.9(5)
C(1)–Mo–C(4)	85.7(6)	C(2)–Mo–C(4)	87.0(6)
C(3)–Mo–C(4)	172.7(6)	Br(1)–Ni–Br(2)	128.9(1)
Br(1)–Ni–P(2)	110.6(1)	Br(2)–Ni–P(2)	111.3(1)
Br(1)–Ni–P(4)	106.4(1)	Br(2)–Ni–P(4)	104.4(1)
P(2)–Ni–P(4)	85.7(1)	O(5)–P(1)–O(7)	98.9(4)
O(5)–P(2)–O(6)	100.6(4)	O(6)–P(3)–O(8)	98.4(4)
O(7)–P(4)–O(8)	100.7(4)	P(1)–O(5)–P(2)	131.7(5)
P(2)–O(6)–P(3)	133.6(5)	P(1)–O(7)–P(4)	132.1(5)
P(3)–O(8)–P(4)	127.8(5)		

$(CO)_4$. Other selected bond distances and angles are presented in Table 5.

Discussion

Formation of $Mo(CO)_4[^iPr_2NPO]_4$ (1). Dithiocarbamate was shown to excise the Mo^{II} vertex selectively from the mixed-valent $Mo(CO)_4[^iPr_2NPO]_4Mo(CO)_2I_2$ complex to give **1** in moderate yield. The unstable orange solid **2** also isolated in this synthesis provided some insight into the mechanism of this reaction. It has IR carbonyl bands at 2018, 1952, 1910, and 1890 cm^{-1}, and its $^{31}P\{^1H\}$ NMR spectrum revealed an ABXY pattern (Tables 1 and 2). Upon standing in solution, it deposited the known red $Mo(CO)_2(S_2CNMe_2)_2$ complex,[7] while the formation of complex **1** could be detected in solution. Similar transformations occurred more slowly in the solid state. Although the elemental analyses for **2** were slightly off, these spectral data suggest that it is most likely the initial metathesis product $Mo(CO)_4[^iPr_2NPO]_4Mo(CO)_2(\eta^1\text{-}S_2CNMe_2)_2$. Rearrangement of the two monodentate dithiocarbamates into chelating modes can then completely dislodge the metal vertex from the cage structure to give **1**.

Structural Comparisons of Complexes 1 and 4c with $Mo(CO)_4[^iPr_2NPO]_4Mo(CO)_4$. Complex **1** represents the third isomer of $Mo(CO)_4[^iPr_2NPO]_4$ we have characterized. It contains the tetraphosphoxane ring in a boat–boat form, in contrast to the chair–boat and chair–chair isomers previously reported.[10] A comparison of molecular structures of monometallic complex **1** and the parent bimetallic $Mo(CO)_4[^iPr_2NPO]_4Mo(CO)_4$ cage can be instructive if significant changes accompany the loss of the Mo vertex.[1] In this case, a shortening of the four P–O bonds at the coordinated part of the heterocycle to 1.623(4) Å has occurred, while those at the demetalated sites are lengthened to 1.671(4) Å. In the parent compound, these eight bonds varied only from 1.642(4) to 1.650(4) Å. In concert, the two O–P–O angles at the coordinated phosphorus atoms have opened up to 102.1(3)°, while the demetalated ones contracted to 97.3(3)°. Similar O–P–O angles were uniformly at 99.1(2)° in the bimetallic cage. Both of these structural changes are consistent with expected enhancement of P–O bonding at the coordinated sites at the expense of the demetalated side.

Recently, a study into the structural alterations within the adamantane-like P_4O_6 framework upon binding of a terminal oxygen or sulfur atom revealed propagation of this disturbance beyond the immediate vicinity into the core structure.[8] For example, at the framework oxygens of the $O{=}P_4O_6$ structure, shortening of P^V–O bonds to 1.594 Å and lengthening of the P^{III}–O bonds to 1.684 Å are observed, while their sums remain about 3.3 Å. The O–P–O angles around P^{III} are also substantially smaller (98.9°) than those at P^V (103.5°). Hence propagation of the $O{=}P^V$ disturbance into the P_4O_6 framework results in a positive charge at the other phosphorus centers while the mediating oxygens suffer little charge displacement. Comparison with the geometries of **1** and other known monometallic tetraphos-

(7) Chen, G. J.-J.; Yelton, R. O.; McDonald, J. W. *Inorg. Chim. Acta* **1977**, *22*, 249. Templeton, J. L.; Ward, B. C. *J. Am. Chem. Soc.* **1980**, *102*, 6568. Young, C. G.; Enemark, J. H. *Aust. J. Chem.* **1986**, *39*, 997.

(8) Muhlhauser, M.; Engels, B.; Marian, C. M.; Peyerimhoff, S. D.; Bruna, P. J.; Jansen, M. *Angew. Chem., Int. Ed. Engl.* **1994**, *33*, 563.

(9) Corbridge, D. E. C. *The Structural Chemistry of Phosphorus*; Elsevier: New York, 1974; Chapters 10 and 11.

(10) Wong, E. H.; Sun, X.; Gabe, E. J.; Lee, F. L.; Charland, J. P. *Organometallics* **1991**, *10*, 3010.

(11) Hudson, H. R. In *The Chemistry of Organophosphorus Compounds*; Hartley, F. R., Ed.; Wiley: New York, 1990; Vol. 1, Chapter 11.

(12) Bodner, G. M.; May, M. P.; McKinney, L. E. *Inorg. Chem.* **1980**, *19*, 1951. Bodner, G. M.; Kahl, S. B.; Bork, K.; Storhoff, B. N.; Wuller, J. E.; Todd, L. J. *Inorg. Chem.* **1973**, *12*, 1071.

(13) Booth, B. L.; Else, M. J.; Fields, R.; Goldwhite, H.; Haszeldine, R. N. *J. Organomet. Chem.* **1968**, *14*, 417. Nesmeynov, A. N.; Isaeva, L. S.; Morozova, L. N. *Inorg. Chim. Acta* **1978**, *29*, L210.

Table 6. Phosphorus–Oxygen Bond Distances and Angles in XP_4O_6 and MP_4O_4 Complexes

	P–O Bond Length (Å)			O–P–O angle (deg)	
compd	at X–P or M–P	at P^{III}	sum	at X–P or M–P	at P^{III}
P_4O_6[a]		1.655	3.310		99.5
OP_4O_6[a]	1.594	1.684	3.278	103.5	98.9
SP_4O_6[a]	1.596	1.678	3.274	103.1	98.9
$Mo(CO)_4[^iPr_2NPO]_4$					
boat–boat, complex **1**	1.623	1.671	3.294	102.1	97.3
chair–chair, chair–boat[b]	1.62	1.70	3.32	99.6	94.3
$PdCl_2[^iPr_2NPO]_4$[b]	1.604	1.674	3.278	102.7	96.2
$PtCl_2[Cy_2NPO]_4$[c]	1.62	1.70	3.32	103.4	96.0

[a] Reference 8. [b] Reference 10. [c] Reference 14.

phoxanes also reveals similar bond length and O–P–O angle trends (Table 6).[8,10,14]

Analogous features in the structure of the Mo/Ni^{II} cage complex **4c** indicate readjustment of the P_4O_4 framework to give very similar [Mo]–P–O and [Ni]–P–O bond lengths averaging 1.65(1) and 1.63(1) Å, respectively. Corresponding O–P–O angles are marginally smaller at the Mo-coordinated sites, ranging from 98.4(4) to 98.9(4)°, compared to 100.6(4)–100.7(4)° at the Ni-bonded sites. Similar trends can also be noted in the known structure of the mixed-valent $Mo(CO)_4[^iPr_2NPO]_4Mo(CO)_2I_2$ complex.[3] Here the [Mo^{II}]–P–O distance of 1.63(1) Å is marginally shorter than the [Mo^0]–P–O lengths of 1.66(1) Å, while the O–P–O angles at Mo^{II} are slightly larger (100°) than those at Mo^0 (98°). These all suggest relaying of electronic effects via the mediating framework oxygens of the MP_4O_4M' core.

The diamagnetism of the palladium analogue of **4c**, $Mo(CO)_4[^iPr_2NPO]_4PdBr_2$ (**4g**), points to a square-planar Pd coordination geometry in contrast to the C_{2v} Ni coordination sphere observed in **4c**. Diamagnetic nickel(II) centers were previously found in a series of $NiBr_2[R_2NPO]_4$ (R = ^{i}Pr, Cy) complexes which featured 1,3-coordination of the P_4O_4 ring in the long-boat form.[6,10] The significantly more congested environment around the nickel vertex of **4c** is most likely responsible for the nonplanar coordination mode and accompanying paramagnetism.

Reactions of Complex 1 with Nucleophiles. Primary alcohols such as methanol and ethanol are found to selectively attack at one of the coordinated phosphorus sites (P(4) in Figure 4). This is reasonable in view of the enhanced electrophilic nature of such P atoms. Cleavage of the P–O–P bond and tautomerization of the resulting P–OH at P(2) to give P(=O)H would then lead to the observed structure of product **3a**. The stereochemistry at P(4) is fully consistent with nucleophilic attack with inversion at this site (Figure 4).

Previously, we have reported that the parent bimetallic cage was completely degraded by piperidine to give diaminophosphine oxide.[4] Similar behavior was observed in the reaction of **1** with piperidine to give cage degradation products, as indicated by a broad ^{31}P NMR doublet at δ −0.40 ($^1J_{PH}$ = 576 Hz). More sterically hindered diisopropylamine attacked these complexes only sluggishly.

Reactions of Complex 1 with Alkylating Agents. Attempted methylation of the free lone pairs in **1** with methyl iodide did not occur in a variety of solvents.

(14) Sun, X.; Wong, E. H.; Jasinski, J. J. Unpublished results.

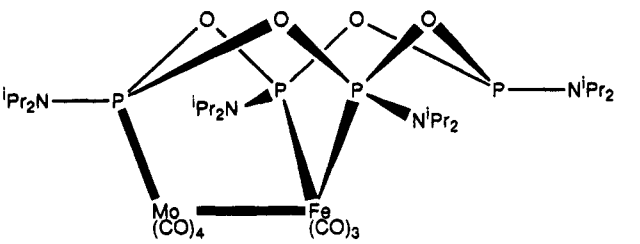

Figure 7. Schematic drawing of a known isomer of complex **4b**, $Mo(CO)_4[^iPr_2NPO]_4Fe(CO)_3$.[6]

Similarly, benzyl bromide did not quaternize these sites. Examination of the structure of **1** suggests serious steric problems associated with any nucleophilic attack by the phosphorus atoms at carbon centers. An additional explanation may lie in the relatively contracted O–P–O angles (97.3(3)°) at these sites. It is well-known that cyclic phosphites with O–P–O angles constrained to less than 100° are retarded in their reactions with electrophiles, as opening up of these angles in the four-coordinate transition state is disfavored.[11]

Formation and Spectral Properties of Heterobimetallic Cage Complexes 4a–g. The convergent lone pairs in complex **1** render it an effective metalla ligand precursor to a variety of heterobimetallic cage complexes. Due probably to steric reasons, the complexation reactions were relatively slow at room temperature and typically required refluxing in hexane to progress satisfactorily. Resulting complexes incorporated additional Cr^0, Fe^0, Ni^0, Cu^I, Ag^I, Ni^{II}, and Pt^{II} vertices (complexes **4a–f**; Scheme 1). All structural and spectral evidence supports their having the same MoP_4O_4M adamantanoid core structure. Coincidentally, a configurational isomer of **4b**, $Mo(CO)_4[^iPr_2NPO]_4Fe(CO)_3$, is now known.[6] With a very different structure, this has an η^3-P_4O_4 ring in a chair–chair conformation bridging the heterometals, which in turn are within bonding distance of each other (Figure 7).

In an interesting departure from the above results, palladium dihalides led instead to MoP_5O_5Pd cage complexes $Mo(CO)_3[^iPr_2NPO]_5PdX_2$ (X = Cl (**5a**), Br (**5b**)) as major isolated products along with smaller amounts of $Mo(CO)_4[^iPr_2NPO]_4Mo(CO)_4$. A speculative net equation can be written to reflect these results (eq 4).

$$6\underset{\mathbf{1}}{Mo(CO)_4[^iPr_2NPO]_4} + 4PdX_2{\cdot}2PhCN \rightarrow 4CO + 4\underset{\mathbf{5a,b}}{Mo(CO)_3[^iPr_2NPO]_5PdX_2} + Mo(CO)_4[^iPr_2NPO]_4Mo(CO)_4 + 8PhCN \quad (4)$$

We have independently prepared an analogue of these products from the reaction of $Mo(CO)_3$(cycloheptatriene) with $PdCl_2[Cy_2NPO]_5$.[6] With shorter reaction times, palladium dibromide did give the expected MoP_4O_4-$PdBr_2$ cage **4g**, along with smaller amounts of **5b** and MoP_4O_4. No indication of the formation of a MoP_4O_4-$PdCl_2$ complex was observed under similarly abbreviated reaction times with $PdCl_2$. Recently we have noted that both the polyphosphoxane ring size and coordination conformation in P_nO_n complexes depend on a fine balance of factors, including the nature of the metal center, its ancillary ligands, and reaction conditions, as well as the P substituent.[6] This represents another

Table 7. $Mo(CO)_4$ a_1 Carbonyl Stretching Frequencies of the Cage Complexes

complex, metal vertices	ν_{CO} (a_1, cm^{-1})
4a, Mo^0/Cr^0	2020.8
$Mo(CO)_4[^iPr_2NPO]_4Mo(CO)_4$, Mo^0/Mo^0	2025.8
4b, Mo^0/Fe^0	2021
6, Mo^0/Ni^0	2022.9
4e, Mo^0/Cu^I	2031.3
4f, Mo^0/Ag^I	2029.7
$Mo(CO)_4[^iPr_2NPO]_4Mo(CO)_2I_2$, Mo^0/Mo^{II}	2035.1
4c, Mo^0/Ni^{II}	2036.7
7a, Mo^0/Ni^{II}	2035.7
7b, Mo^0/Ni^{II}	2037.4
4g, Mo^0/Pd^{II}	2045.8
4d, Mo^0/Pt^{II}	2045.1

Table 8. ^{13}C NMR Data (ppm) for the $Mo(CO)_4$ Moiety of the Cage Complexes

complex, metal vertices	δ(cis)	δ(trans)	av
4a, Mo^0/Cr^0	207.2	218.0	212.6
$Mo(CO)_4[^iPr_2NPO]_4Mo(CO)_4$, Mo^0/Mo^0	207.3	213.9	210.6
4b, Mo^0/Fe^0	207.7	217.3	212.5
6, Mo^0/Ni^0	208.0	215.0	211.5
4e, Mo^0/Cu^I	207.2	213.3	210.2
4f, Mo^0/Ag^I	207.5	213.2	210.4
$Mo(CO)_4[^iPr_2NPO]_4Mo(CO)_2I_2$, Mo^0/Mo^{II}	206.2	211.0	208.6
4g, Mo^0/Pd^{II}	205.1	211.8	208.4
4d, Mo^0/Pt^{II}	205.1	212.1	208.6

example of the subtle shifts in reaction course within the same family of metal precursors.

Isolation of complex **4g**, $Mo(CO)_4[^iPr_2NPO]_4PdBr_2$, allowed us to observe its thermal reaction with a $^iPr_2N-P{=}O$ source to see if it can serve as an intermediate to the MoP_5O_5Pd cage **5b**. Indeed, **5b** was the major product formed in the reaction of **4g** with $(^iPr_2N)_2P(O)H$.

The well-resolved higher frequency a_1 carbonyl stretching band of the conserved *cis*-$Mo(CO)_4$ moiety in all these MoP_4O_4 cage complexes provides a sensitive gauge of possible intracage effects.

A tabulation of these values for the P_4O_4 complexes now available to us reveals a small but possibly significant dependence on the oxidation state of the cross-cage metal center (Table 7). The presence of a second zerovalent metal center resulted in the frequency range of 2021−2026 cm^{-1}. Introduction of monovalent metal vertices produced values of 2030−2031 cm^{-1}, while divalent centers resulted in the highest stretching frequencies observed at 2035−2046 cm^{-1}. This trend appears to reflect the increasing electronic demands at the second metal site being transmitted to the $Mo(CO)_4$ vertex. For support of this postulate, the molybdenum carbonyl ^{13}C NMR shifts were also examined (Table 8). Indeed, the average CO δ values for these species also revealed an upfield shift with increasing formal charge at the second site. Previously, such trends have been correlated to reflect decreasing electron density at the Mo center.[12] Since both the IR and NMR shifts observed are relatively small and may well be sensitive to steric as well as electronic influences, a broader range of structural and spectral data may be needed to affirm this premise.

(15) King, R. B. *Organometallic Synthesis*; Academic Press: New York, 1965; Vol. 1, p 122.

Synthesis and Halogenation Reactions of Complex 6. Precedents exist for the use of iron pentacarbonyl or diiron nonacarbonyl as reducing and carbonylating agents.[13] Thus, we found that both were effective in converting $Mo(CO)_4[^iPr_2NPO]_4NiX_2$ (X = Cl (**7a**), I (**7b**)) to the diamagnetic $Mo(CO)_4[^iPr_2NPO]_4Ni(CO)_2$ cage **6**, presumably with formation of FeX_2 (eq 5).

$$Mo(CO)_4[^iPr_2NPO]_4NiX_2 + Fe(CO)_5 \xrightarrow[\mathbf{7a,b}]{} Mo(CO)_4[^iPr_2NPO]_4Ni(CO)_2 + FeX_2 + 3CO \quad (5)$$
$$\mathbf{6}$$

Competitive iodination or chlorination of this Mo^0/Ni^0 cage resulted in exclusive halogenation at the Ni site, as only the $Ni(CO)_2$ carbonyl IR stretches disappeared with concurrent formation of the respective $Mo(CO)_4[^iPr_2NPO]_4NiX_2$ derivatives (**7a,b**) (eq 3).

Summary

We have shown that it is possible to selectively remove the Mo^{II} vertex from the core of the mixed-valent $Mo^0P_4O_4Mo^{II}$ complex without destroying the remainder of the cage framework. The stable product $Mo(CO)_4[^iPr_2NPO]_4$ has been characterized spectrally and structurally and its reaction chemistry with several nucleophiles and alkylating agents examined. The presence of convergent phosphorus lone pairs in this metallaligand allowed the syntheses of a series of heterobimetallic $Mo^0P_4O_4M$ complexes. Spectral and structural studies confirmed reconstitution of the admantanoid core in these products. Some spectral evidence for intracage transmission of metal−metal influence is presented. The preparation of this series of complexes represents a rare example of selective vertex substitution in cage structures of the adamantane family.

Experimental Section

All manipulations were performed using standard inert-atmosphere techniques. Solvents were dried and distilled under nitrogen before use. Methylene chloride and hexanes were from CaH_2, and toluene was from sodium. Sulfuryl chloride, $Fe(CO)_5$, $Fe_2(CO)_9$, and sodium dimethyldithiocarbamate were all purchased from the Aldrich Chemical Co. $Cr(CO)_4(NBD)$,[15] $(AgNO_3)_2(NBD)$,[16] $NiBr_2$·DME,[17] $PtCl_2(NBD)$,[18] $Cu(CH_3CN)_4BF_4$,[19] $PdCl_2$·2PhCN,[20] and $PdBr_2$·2PhCN[21] were all prepared by published procedures. The $Mo(CO)_4[^iPr_2NPO]_4Mo(CO)_2I_2$ complex was synthesized as described previously.[3]

^1H, ^{13}C, and ^{31}P NMR spectra were obtained on a JEOL FX-90Q or a Bruker AM-360 spectrometer. Proton and carbon shifts were referenced to internal TMS, while ^{31}P shifts were referenced to external 85% H_3PO_4. ^{13}C and ^1H NMR data are summarized in Tables 9 and 10, respectively. Infrared spectra were recorded on a Perkin-Elmer 283B and a Nicolet MX-1 FT-IR instrument using KBr disks. Elemental analyses were performed at the University of New Hampshire Instrumentation Center on a Perkin-Elmer 2400 elemental analyzer.

(16) Abel, E. W.; Bennett, M. A.; Wilkinson, G. *J. Chem. Soc.* **1959**, 3178.
(17) Ward, L. G. L. *Inorg. Synth.* **1972**, *13*, 154.
(18) Drew, D.; Doyle, J. R. *Inorg. Synth.* **1990**, *28*, 346.
(19) Kubas, G. J. *Inorg. Synth.* **1990**, *28*, 68.
(20) Doyle, J. R.; Slade, P. E. *Inorg. Synth.* **1960**, *6*, 218.
(21) McCrindle, R.; Alyea, E. C.; Ferguson, G.; Dias, S. A.; McAlees, J.; Parvez, M. *J. Chem. Soc., Dalton Trans.* **1980**, 137.

Table 9. ^{13}C NMR Data for the Cage Complexes[a]

complex	chem shift, ppm (assignt, J_{CP} in Hz)
1	215.8 (t, CO, J = 14), 209.5 (t, CO, J = 12), 48.0 (t, NC, J = 7), 44.3 (t, NC, J = 8), 24.2 (s, Me), 23.2 (s, Me)
2	241.1 (m, S_2C), 215.0 (m, CO), 210.0 (bd, CO), 209.1 (bd, CO), 207.2 (bd, CO), 48.3 (bd, s), 47.8 (bd, s), 46.9 (bd, s), 39.4 (s, NMe_2), 24.2 (bd, $NCH(CH_3)_2$)
3a	214.7 (d of d, CO, J = 12, 18), 214.2 (t, CO, J = 14), 209.4 (m, CO), 208.7 (t, CO, J = 12), 51.3 (s, POMe), 49.0 (d, NCH, J = 14), 48.2 (d, NCH, J = 11), 45.4 (d, NCH, J = 6), 44.6 (d, NCH, J = 15), 24.3−22.9 (m, Me)
3b	214.1 (d of d, CO, J = 7, 11), 213.6 (t, CO, J = 11), 208.8 (m, CO), 207.9 (t, CO, J = 12), 60.4 (s, $POCH_2$), 48.7 (d, NCH, J = 14), 47.9 (d, NCH, J = 11), 45.1 (d, NCH, J = 6), 44.3 (d, NCH, J = 14), 24.1−22.8 (m, Me), 15.7 (d, P-OCH_2CH_3, J = 9)
4a	224.5 (t, CO, J = 9), 218.0 (t, CO, J = 18), 214.0 (t, CO, J = 16), 207.2 (t, CO, J = 13), 47.0 (t, NC, J = 7), 46.8 (t, NC, J = 5), 24.3 (s, Me), 24.0 (s, Me)
4b	217.3 (t, CO, J = 7), 214.5 (t, CO, J = 15), 207.6 (t, CO, J = 13), 48.1, 47.7 (t, NC, J = 6, 7), 24.1 and 24.0 (s, Me's)
4c	paramagnetic
4d	212.1 (t, CO, J = 17), 205.1 (t, CO, J = 12), 48.2 (t, NC, J = 6), 47.3 (t, NC, J = 3), 23.9 and 23.6 (s, Me's).
4e	213.3 (t, CO, J = 16), 207.2 (t, CO, J = 12), 120.4 (s, *C*N), 48.3 (t, NC, J = 6), 45.3 (t, NC, J = 6), 23.6 and 23.1 (s, Me's), 2.2 (s, CH_3CN)
4f	213.2 (t, CO, J = 16), 207.5 (t, CO, J = 12), 48.6 and 45.4 (t, NC, J = 6 and 7), 23.9 and 23.1 (s, Me's)
4g	211.8 (m, CO), 205.1 (t, CO, J = 13), 48.6 (t, NC, J = 6), 48.2 (t, NC, J = 3), 24.0 (s, Me)
5a	218.1 (d of t, CO, J = 39, 14), 216.1 (d of t, J = 41, 10), 50.2 (t, NC, J = 6), 48.8 and 48.5 (d's, NC, J = 15, 12), 25.1−23.2 (Me)
5b	218.2 (d of t, CO, J = 39, 14), 216.3 (d of t, CO, J = 41, 10), 50.2 (t, NC, J = 5), 48.7 (d, NC, J = 15), 48.3 (d, NC, J = 12), 25.2− 23.0 (Me)
6	215.0 (CO, J = 15), 208.2 (t, CO, J = 12 Hz), 48.0 (t, NC, J = 6), 46.3 (t, NC, J = 6), 23.7 and 23.6 (Me)
7a	paramagnetic
7b	paramagnetic

[a] All spectra were run in $CDCl_3$ solutions, except for **6**, which was in C_6D_6 (t = triplet, d = doublet, s = singlet, bd = broad).

Table 10. Proton NMR Data for the Cage Complexes[a]

complex	chem shift, ppm (multiplicity, assignt, J in Hz)
1	4.01 (septet, NCH, J = 6.8), 3.77 (bd, NCH), 1.30 and 1.12 (d, Me, J = 6.8)
2	4.50 (bd, NCH), 4.31 (septet, NCH, J = 6.5), 3.4 and 3.3 (bd, NMe), 1.3 (bd, NCH*Me*)
3a	7.50 (d, P(O)H, J_{PH} = 635.2), 4.34, 3.96, 3.47 (septets, NCH, J = 6.8, 7.1, 6.4), 3.41 (d, POMe, J = 12.4), 3.36 and 3.32 (septets, NCH, J = 6.7) 1.51 (d, NCH*Me*, J = 6.8), 1.27−1.12 (m, Me)
3b	7.58 (d, P(O)H, J_{PH} = 634.9), 4.35 (septet, NCH, J = 6.9), 3.97 (m, NCH and $POCH_2$), 3.54, 3.35, 3.34 (septets, NCH, J = 5.9, 6.8, 6.7), 1.46 (d, NCH*Me*, J = 6.8), 1.27 (m, NCH*Me* and $POCH_2$*Me*)
4a	4.47 and 4.14 (septets, NCH, J = 7.0), 1.29 ("triplet", Me, J = 7.0)
4b	4.38 and 4.27 (septets, NCH, J = 7.0), 1.30 (multiplet, Me)
4c	paramagnetic
4d	4.30 and 3.69 (septets, NCH, J = 6.9), 1.46 and 1.40 (doublets, Me, J = 6.9)
4e	4.03 and 3.83 (septets, NCH, J = 7.1), 2.35 (s, MeCN), 1.29 (doublet, Me, J = 7.1)
4f	3.99 and 3.83 (septets, NCH, J = 6.8), 1.28 (doublets, Me, J = 6.8)
4g	4.29 and 3.79 (septets, NCH, J = 7.3, 6.8), 1.48 and 1.45 (doublets, Me, J = 7.2 and 6.8)
5a	4.64, 4.16, 4.14 (septets, NCH, J = 6.9, 7.2, 7.1), 1.43−1.40 (m, Me), 1.32 (d, Me, J = 6.9)
5b	4.68, 4.18, 4.14 (septets, NCH, J = 6.7, 7.1, 6.7) 1.42−1.38 (m, Me), 1.33 (d, Me, J = 6.9)
6	4.04, 3.97 (septets, NCH, J = 7.1, 7.0)), 1.30, 1.27 (d, Me, J = 7.0, 7.1)
7a	paramagnetic
7b	paramagnetic

[a] All spectra were run in $CDCl_3$ solutions except for **6**, which was in C_6D_6 (m = multiplet, d = doublet, bd = broad)

$Mo(CO)_4[^iPr_2NPO]_4$ (1) and $Mo(CO)_4[^iPr_2NPO]_4Mo(CO)_2(S_2CNMe_2)_2$ (2). A 250 mL round-bottomed flask with a magnetic stirbar was charged with 5.00 g of $Mo(CO)_4[^iPr_2NPO]_4Mo(CO)_2I_2$ (4.16 mmol) and 1.25 g (8.40 mmol) of sodium dimethyldithiocarbamate. A 100 mL amount of CH_2Cl_2 was added to dissolve the mixed-valent complex, resulting in a burgundy red suspension. After the mixture was stirred for 3 h at room temperature, TLC (15% ethyl acetate in hexane, neutral alumina) revealed a colorless and a yellow component. Filtration yielded a red-purple solid identified as $Mo(CO)_2[S_2CNMe_2]_2$ (IR, CHN analysis) and a red solution. Evaporation of the filtrate gave a red solid which was allowed to stand at room temperature for 1 week. This residue was then extracted three times with hexane to give an orange-yellow extract solution. After evaporation, the residue was chromatographed on an alumina column using 15% ethyl acetate in hexane eluant. First to elute was the colorless complex **1**, which was isolated in 60% yield (1.95 g). Next to elute was the unstable orange complex **2** (0.87 g). Anal. Calcd for **1**, $C_{28}H_{56}MoN_4O_8P_4$: C, 42.2; H, 7.10, N, 7.03. Found: C, 42.00; H, 7.10; N, 6.91. Anal. Calcd for **2**, $C_{36}H_{68}Mo_2N_6O_{10}P_4S_4$: C, 36.36; H, 5.76; N, 7.10. Found: C, 36.34; H, 6.30; N, 6.68.

$Mo(CO)_4[(^iPr_2NPO)_2(^iPr_2NPOMe)\{^iPr_2NP(O)H\}]$ (3a). Method A. A 0.402 g (0.335 mmol) amount of $Mo(CO)_4[^iPr_2NPO]_4Mo(CO)_2I_2$ and 0.0959 g (0.669 mmol) of sodium dimethyldithiocarbamate in 20 mL of methylene chloride was stirred to give a burgundy red suspension. Addition of 10 mL of methanol gave a deep red solution, which was stirred for 3 h. The reaction mixture was filtered to remove $Mo(CO)_2(S_2CNMe_2)_2$ (0.0834 g), and the filtrate was evaporated to a red-brown residue. This was extracted with 20 mL of hexane, and from the extract was obtained 0.210 g (70%) of white solid **3a**.

Method B. A 0.339 g (0.426 mmol) amount of **1** was dissolved in 6 mL of methanol and 4 mL of hexane and the mixture stirred for 9 h. The clear, light yellow solution was evaporated to dryness to give a light yellow solid. This was resuspended in 5 mL of methanol and filtered. The residue was washed twice with 1 mL of cold hexane and then dried to give 0.264 g (75%) of white complex **3a**. Recrystallization from hot hexane gave X-ray-quality crystals. Anal. Calcd for $C_{29}H_{60}MoN_4O_9P_4$: C, 42.02; H, 7.31; N, 6.76. Found: C, 41.74; H, 7.62; N, 6.77.

$Mo(CO)_4[(^iPr_2NPO)_2(^iPr_2NPOEt)\{^iPr_2NP(O)H\}]$ (3b). A 25 mL flask with stirrer was charged with 0.695 g of complex **1** (0.872 mmol), 10 mL of absolute ethanol, and 4 mL of hexane. After reflux for 24 h, the light orange solution was cooled and concentrated to ~5 mL to give a suspension which was filtered to give about 0.1 g of a white solid identified as unreacted **1**. Addition of 4 mL of ethanol led to the precipitation of **3b**, which was filtered off, washed twice with 2 mL of ethanol, and dried

to give 0.452 g (72% based on reacted **1**) of complex **2**. Anal. Calcd for $C_{30}H_{62}MoN_4O_9P_4$: C, 42.75; H, 7.41; N, 6.65. Found: C, 42.59; H, 7.64; N, 6.51.

$Mo(CO)_4[^iPr_2NPO]_4Cr(CO)_4$ (4a). A 1.52 g (1.91 mmol) amount of **1** and 0.918 g (3.82 mmol) of $Cr(CO)_4(NBD)$ was refluxed in 40 mL of hexane for 3 days. After evaporation of volatiles under reduced pressure, the bright yellow residue was washed three times with 10 mL of hexane to give a light yellow solid. This was chromatographed on alumina using 5% ethyl acetate in hexane as the eluant to give the colorless solid **4a** (0.58 g, 35%). Anal. Calcd for $C_{32}H_{56}CrMoN_4O_{12}P_4$: C, 40.01; H, 5.88; N, 5.83. Found: C, 40.31; H, 6.06; N, 5.74.

$Mo(CO)_4[^iPr_2NPO]_4Fe(CO)_3$ (4b). A 2.83 g (3.55 mmol) amount of **1** and 1.75 g (9.59 mmol) of $Fe_2(CO)_9$ was refluxed in 60 mL of hexane for 40 h. The cooled reaction mixture was stripped of volatiles and chromatographed on an alumina column using 2% ethyl acetate in hexane eluant to give 0.94 g (30%) of **4b** as a white solid. Anal. Calcd for $C_{31}H_{56}FeMoN_4O_{11}P_4$: C, 39.76; H, 6.03; N, 5.98. Found: C, 39.50; H, 6.30; N, 6.04.

$Mo(CO)_4[^iPr_2NPO]_4NiBr_2$ (4c). A 1.20 g (1.51 mmol) amount of **1** and 0.400 g (1.51 mmol) of $NiBr_2$·DME was refluxed in 20 mL of hexane for 5 h. The brown-red suspension was concentrated to about 5 mL, and the red crystalline precipitate was filtered, washed twice with 5 mL of cold hexane, and dried to give 1.23 g (80%) of complex **4c**. Anal. Calcd for $C_{28}H_{56}Br_2MoN_4NiO_8P_4$·0.7(hexane): C, 35.95; H, 6.17; N, 5.21. Found: C, 35.92; H, 6.24; N, 5.31. X-ray-quality crystals were grown from a hot hexane solution.

$Mo(CO)_4[^iPr_2NPO]_4PtCl_2$ (4d). A 0.306 g (0.384 mmol) amount of **1** and 0.138 g (0.384 mmol) of $PtCl_2(NBD)$ was heated to 60 °C in 10 mL of toluene for 4 h. After cooling and filtration, a white solid was obtained. This was washed with toluene and dried to give 0.359 g (88%) of complex **4d**. Anal. Calcd for $C_{28}H_{56}Cl_2MoN_4O_8P_4Pt$: C, 31.65; H, 5.31; N, 5.27. Found: C, 31.94; H, 5.45; N, 5.36.

$Mo(CO)_4[^iPr_2NPO]_4Cu(MeCN)_2BF_4$ (4e). A 0.117 g (0.147 mmol) amount of **1** and 0.023 g (0.073 mmol) of $Cu(MeCN)_4BF_4$ was refluxed in 8 mL of hexane and 4 mL of CH_2Cl_2 for 1 h. After evaporation of most of the CH_2Cl_2, the reaction suspension was refluxed another 3 h. Filtration gave a white solid, which was washed with hexane and dried to give 0.072 g (95% based on Cu) of **4e**. Anal. Calcd for $C_{32}H_{62}BCuF_4MoN_6O_8P_4$: C, 37.35; H, 6.07; N, 8.16. Found: C, 37.10; H, 6.16; N, 7.55.

$Mo(CO)_4[^iPr_2NPO]_4AgNO_3$ (4f). A 0.440 g (0.552 mmol) amount of **1** and 0.0592 g (0.276 mmol) of $(NBD)(AgNO_3)_2$ was stirred in 20 mL of hexane in the absence of light. After 1 h, the white suspension was filtered and the solid washed with hexane and dried to give 0.243 g (54%) of complex **4f**. Satisfactory elemental analyses were not obtained due to its instability.

$Mo(CO)_3[^iPr_2NPO]_5PdCl_2$ (5a). A 0.712 g (0.894 mmol) amount of **1** and 0.274 g (0.715 mmol) of $PdCl_2$·2PhCN in 20 mL of toluene was heated to 70 °C for 66 h. The resulting red suspension was cooled to room temperature and filtered to give 0.421 g of a gray-yellow solid and a red-brown solution. The solid was dissolved in 8 mL of chloroform, the solution filtered, and the filtrate allowed to evaporate slowly. A total of 0.345 g of yellow needles of **5a** was obtained. The red-brown filtrate was evaporated to dryness and the residue washed three times with 2 mL of acetone to give a yellow solid which was a 2:1 mixture of **5a** and $Mo(CO)_4[^iPr_2NPO]_4Mo(CO)_4$ by ^{31}P NMR. This mixture was washed three times with small amounts of hexane to give additional **5a**, for a combined yield of 0.504 g (52% based on Pd). Anal. Calcd for $C_{33}H_{70}Cl_2MoN_5O_8P_5Pd$: C, 36.26; H, 6.41; N, 6.46. Found: C, 36.27; H, 6.48; N, 6.10.

$Mo(CO)_3[^iPr_2NPO]_5PdBr_2$ (5b). A 0.684 g (0.958 mmol) amount of **1** and 0.324 g (0.686 mmol) of $PdBr_2$·2PhCN in 20 mL of toluene were heated to 70 °C for 72 h. The yellow-brown suspension was cooled to room temperature and filtered to give a grayish yellow solid and a clear brown filtrate. The residue was dissolved in 4 mL of chloroform, the solution filtered, and the filtrate allowed to evaporate slowly. Yellow crystals of **5b** formed and were collected and dried (0.400 g). The brown filtrate was evaporated to a brown residue, which was found by ^{31}P NMR to be a 1:2:4 mixture of $Mo(CO)_4[^iPr_2NPO]_4Mo(CO)_4$, **4g**, and **5b**. It was washed twice with 5 mL of a 1:1 mixture of acetone and hexane, followed by 2 × 2 mL of hexane to give 0.124 g of **5b**. The combined yield is 48% based on Pd. Anal. Calcd for $C_{33}H_{70}Br_2MoN_5O_8P_5Pd$: C, 33.53; H, 5.97; N, 5.93. Found: C, 33.88; H, 6.33; N, 5.83.

Table 11. Crystallographic Data for Complexes 1, 3a, and 4c

	4c	1	3a
	(a) Crystal Parameters		
formula	$C_{28}H_{56}Br_2MoN_4NiO_8P_4$	$C_{28}H_{56}MoN_4O_8P_4$	$C_{29}H_{60}MoN_4O_9P_4$
fw	1015.1	796.5	828.6
cryst syst	monoclinic	tetragonal	monoclinic
space group	*C*2/*c*	$P4_2/mnm$	$P2_1/c$
a, Å	20.339(3)	18.028(5)	21.734(9)
b, Å	13.204(2)		11.914(3)
c, Å	35.484(7)	14.003(4)	16.845(6)
β, deg	93.45(2)		91.92(3)
V, Å^3	9512(3)	4551(2)	4359(3)
Z	8	4	4
cryst dimens, mm	0.20 × 0.20 × 0.46	0.33 × 0.34 × 0.40	0.32 × 0.32 × 0.51
cryst color	dark red	colorless	colorless
D(calc), g cm^{-3}	1.418	1.162	1.263
μ(Mo Kα), cm^{-1}	25.06	4.63	4.94
temp, K	299	297	296
T(max)/*T*(min)			1.032
	(b) Data Collection		
diffractometer	Siemens P4		
monochromator	graphite		
radiation	Mo Kα (*λ* = 0.710 73 Å)		
2*θ*, scan range, deg	4.0−45.0	4.0−50.0	4.0−52.0
data collected (*hkl*)	±21,+14,+38	+21,+21,+16	±26,+14,+20
no. of rflns collected	6642	4162	7520
no. of indpt rflns	6199	2194	7339
R(merg), %	6.13	3.51	1.79
no. of indpt obsd rflns, $F_o \geq n\sigma(F_o)$	3253 (*n* = 4)	1460 (*n* = 5)	4978 (*n* = 4)
std rflns	3 std/197 rflns	3 std/197 rflns	3 std/197 rflns
var in stds., %	14	5	<1
	(c) Refinement		
R(*F*), %	6.03	5.59	4.43
R(w*F*), %	7.54	8.44	5.25
Δ/*σ*(max)	0.152	0.408	0.002
Δ(*ρ*), e Å^{-3}	0.87	0.50	0.60
N_o/N_v	7.4	10.2	11.6
GOF	1.08	1.23	1.07

$Mo(CO)_4[^iPr_2NPO]_4PdBr_2$ (4g). A 0.427 g (0.536 mmol) amount of **1** and 0.251 g (0.487 mmol) of $PdBr_2$·2PhCN in 20 mL of toluene was heated to 70 °C for 16 h. After cooling and removal of volatiles, a yellow-brown residue remained. This was washed three times with 5 mL of hexane to give 0.449 g of a greenish yellow solid. The solid was dissolved in 5 mL of chloroform, the solution filtered, and the clear yellow solution evaporated to give 0.432 g of **4g** (83% based on Pd). A hot toluene solution of this gave crystals upon cooling and slow evaporation. Anal. Calcd for $C_{28}H_{56}Br_2MoN_4O_8P_4Pd$: C, 31.64; H, 5.31; N, 5.27. Found: C, 31.71; H, 5.32; N, 5.18.

$Mo(CO)_4[^iPr_2NPO]_4Ni(CO)_2$ (6). A 0.64 g (0.63 mmol) amount of **4c** and 0.50 mL (3.8 mmol) of $Fe(CO)_5$ in 10 mL of hexane was stirred at room temperature for 2 h to give a yellow suspension. After filtration and evaporation of volatiles from the filtrate, the yellow residue was chromatographed on alumina using 5% ethyl acetate in hexane to give 0.49 g (85% based on **4c**) of white complex **6**. Anal. Calcd for $C_{30}H_{56}MoN_4NiO_{10}P_4$: C, 39.53; H, 6.19; N, 6.15. Found: C, 39.40; H, 6.23; N, 6.05.

$Mo(CO)_4[^iPr_2NPO]_4NiCl_2$ (7a). A 0.320 g (0.351 mmol) amount of **6** in 20 mL of hexane was cooled to −78 °C. A solution of 0.390 mL (4.86 mmol) of SO_2Cl_2 in 40.0 mL of

methylene chloride was made, and 3.18 mL of this was added dropwise to the hexane solution of **6**. The clear solution turned yellow, and within 5 min, an orange suspension then formed. The reaction mixture was concentrated to half its volume, filtered, and dried to give 0.273 g (84%) of **7a** as an orange solid. Anal. Calcd for $C_{28}H_{56}Cl_2MoN_4NiO_8P_4$: C, 36.31; H, 6.09; N, 6.05. Found: C, 36.54; H, 6.50; N, 5.54.

$Mo(CO)_4[^iPr_2NPO]_4NiI_2$ (7b). A 0.154 g (0.169 mmol) amount of **6** was dissolved in 5 mL of CH_2Cl_2. A solution of 0.472 g (0.186 mmol) of iodine in 2 mL of CH_2Cl_2 was added and the mixture stirred for 2 h to give a deep red solution. This was evaporated to dryness under reduced pressure to give a dark red residue. Washing twice with 1 mL of acetonitrile and drying gave 0.142 g (76%) of **7a**. Satisfactory elemental analyses were not obtained due to its instability.

Crystallographic Studies. Crystal, data collection, and refinement parameters are given in Table 11. Single crystals of **1**, **3a**, and **4c** were grown from saturated hexane solutions of the respective compounds. Suitable crystals were selected and mounted on glass fibers with epoxy cement. In each case, unit cell parameters were obtained by least-squares refinement of the angular settings of 25 reflections ($20° \leq 2\theta \leq 25°$). The XABS program was used to correct the data of **4c** for absorption;[22] corrections were also performed to compensate for 14% linear decay in check reflection intensities. A semiempirical ellipsoid correction was applied to the data set of **3a**.

Systematic absences in the diffraction data for **4c** are consistent for space groups *C*2/*c* and *Cc*, for **1**, $P4_2/mnm$, $P4_2nm$, and *P*4*n*2, and uniquely for **3a**, $P2_1/c$. The *E* statistics suggested the centrosymmetric alternatives for **4c** and **1**, and these space groups were verified by subsequent refinements.

The molecule in **1** is located along an axis with 4-fold symmetry. The isopropyl groups attached to N(2) were disordered and occur in several positions. In both **4c** and **1**, several peaks on the Fourier difference maps, not connected with the metal complexes, were observed. Attempts to model these as chemically identifiable solvent molecules were unsuccessful. These apparent solvent molecules were assigned carbon identities and isotropically refined.

All structures were solved by direct methods, completed by subsequent difference Fourier syntheses, and refined by full-matrix least-squares procedures. All non-hydrogen, non-solvent atoms were refined with anisotropic displacement coefficients. Hydrogen atoms were treated as idealized contributions. All software and sources of the scattering factors are contained in either the SHELXTL (5.1) or SHELXTL PLUS (4.2) program libraries (G. Sheldrick, Siemens XRD, Madison, WI).

Acknowledgment. We acknowledge financial support from the donors of the Petroleum Research Fund, administered by the American Chemical Society.

Supplementary Material Available: Listings of atomic coordinates, anisotropic thermal factors, and bond lengths and angles for **1**, **3a**, and **4c** (16 pages). Ordering information is given on any current masthead page.

OM940471S

(22) Hope, H.; Moezzi, B. University of California, Davis, CA.